GEOLOGICAL SURVEY OF CANADA

OPEN FILE 1998

THE LIME HILL GNEISS – A BASEMENT IN THE BRAS D'OR ZONE OF CAPE BRETON ISLAND

Robert P. Raeside
Department of Geology
Acadia University
Wolfville, Nova Scotia
B0P 1X0

Canada

1989

GEOLOGICAL SURVEY OF CANADA
OPEN FILE 1998

THE LIME HILL GNEISS – A BASEMENT IN THE BRAS D'OR ZONE OF CAPE BRETON ISLAND

Robert P. Raeside
Department of Geology
Acadia University
Wolfville, Nova Scotia
B0P 1X0

Abstract

The Lime Hill gneissic complex of the Bras d'Or Zone of Cape Breton Island contains migmatitic paragneisses, orthogneiss, amphibolite and calc-silicate metamorphic rocks. The dominant lithologies are biotite and biotite-cordierite gneisses, which have been metamorphosed to upper amphibolite facies conditions. Based on analysis of phase relationships, the cordierite-K-feldspar-sillimanite anatectic migmatites have formed at temperatures above 650°C and pressures below 400 MPa. Geothermobarometry yields conditions of about 750°C and 350 MPa. Minor spinel- and corundum-bearing neosomes in the migmatites indicate similar temperature and pressure conditions. This first metamorphism is interpreted to be related to that displayed by the Kellys Mountain Gneiss, and appears to be distinctive of the gneisses of the Bras d'Or Zone. Extensive retrograde metamorphism, which was probably related to younger intrusive events (dyke or alkali feldspar granite intrusions) occurred at lower amphibolite facies conditions, in the andalusite stability field.

Introduction

Cape Breton Island can be divided into tectonostratigraphic zones which represent a compressed section of the Appalachian Orogen (Fig. 1). These are bounded to the north by the Grenvillian rocks of the Northwestern Highlands, and to the southeast by the Avalonian rocks of the Southeastern Zone, which in turn are juxtaposed against the Meguma Zone, across the Cobequid-Chedabucto Fault System (Barr and Raeside 1986).

The central part of Cape Breton Island is underlain by the Bras d'Or Zone, a belt characterized by a number of basement blocks in which occur Precambrian rocks of the George River Group, including quartzite, greywacke, slate, marble and minor mafic volcanic rocks in at least five widely separated areas (Milligan 1970). Other significant units in the Bras d'Or Zone include compositionally expanded Hadrynian to Cambrian I-type granitoid suites, and Middle Cambrian to Ordovician sedimentary units (Bourinot Group) both of which are also characteristic of the Southeastern Zone (Barr and Raeside 1986). Intruded into the Bras d'Or Zone are large plutons of apparent Ordovician age (Barr and Setter 1984, Barr *et al* 1982, 1985), which bear similarities to plutons ascribed to the Aspy and Ingonish Zones, and overlying the lower Paleozoic and Precambrian rocks of the western Bras d'Or Zone are Devonian volcanic rocks of the Fisset Brook Formation, which are also found in the zones to the north. The Bras d'Or Zone, therefore, in many respects appears transitional between the recognized Avalonian rocks of southeastern Cape Breton Island, and the less well understood, but higher grade and more severely deformed rocks with possible Grenvillian affinities in northern Cape Breton Island.

The diagnostic unit of the Bras d'Or Zone is the George River Group. Although rocks assigned to this group have in the past been described from large areas of northern and central Cape Breton Island (e.g. Milligan 1970,

Wiebe, 1972, Keppie 1979), detailed mapping has limited the known extent of the unit to the Bras d'Or Zone (Raeside *et al.* 1984, Barr *et al.* 1985, Raeside *et al.* 1986, Raeside and Barr 1986, Barr *et al.* 1987b, Raeside and Barr 1987). Typically the rocks of the George River Group are at low metamorphic grade, except where they have been intruded by post-metamorphic plutons.

Areas of higher metamorphic grade gneiss and schist also occur in the Bras d'Or Zone, the most extensively studied of which is the Kellys Mountain Gneiss which outcrops along the Trans-Canada Highway (Barr *et al.* 1982, Jamieson 1984). Other portions of gneiss have been reported from the Boisdale Peninsula (Barr and Setter 1984), the North Mountain area at Lime Hill (Justino and Sangster 1987), and the Creignish Hills at Whycocomagh (Campbell, in preparation), although no detailed studies have been conducted on these units. The Kellys Mountain Gneiss has been investigated by Jamieson (1984) who reported the occurrence of low pressure cordierite-bearing migmatites which equilibrated under peak metamorphic conditions of 100 to 350 MPa and 580-700°C. She inferred it to have formed under conditions of an abnormally high geothermal gradient associated with the intrusion of diorites.

Geologic setting and field relations of the North Mountain

The area of the North Mountain has been mapped by Kelley (1967) who in common with many earlier workers in central Cape Breton Island (e.g. Guernsey 1928, Bell and Goranson 1938) assigned all the metasedimentary and gneissic rock types in the block to the George River Group (*sensu lato*). These include low grade phyllites, greenschists and crystalline limestones of the George River Group (*sensu stricto*) as well as higher grade gneisses and marbles. Milligan (1970) included much of the area now recognized as the Lime Hill gneissic complex as Paleozoic granite, with those portions associated with carbonate rocks as interstratified marble and gneiss. He was unable to

determine the relation between the gneiss and the adjacent low grade rocks of the George River Group (*sensu stricto*) to the north.

Chatterjee (1977, 1980a, 1980b) described the mineralization at the Lime Hill zinc and tungsten showing, and based on the known distribution of calc-silicate and carbonate rocks inferred them to occur as roof pendants in felsic intrusive rocks. By analysis of the phase relationships of calc-silicate minerals and the host rock mineralization he also proposed a contact metamorphic origin for both the mineralization and the peak metamorphism of the metasedimentary rocks.

Most recently, the North Mountain has been mapped in detail by Justino (1985) and the Lime Hill zinc showing has been described by Justino and Sangster (1987). They recognized that low grade George River Group rocks *sensu stricto* exist north of a fault extending across the North Mountain, and that higher grade gneisses, amphibolites and carbonate-bearing rocks exist south of the fault. They also indicated that these high grade rocks were more extensive than previously recognized, and include a portion of gneisses on the southwestern side of the North Mountain. They did not consider these high grade rocks to be part of the George River Group *sensu stricto* and described them as the Lime Hill gneissic complex. Intruded into the Lime Hill gneissic complex are granodiorite (526 ± 21 Ma, K-Ar, hornblende, M. Justino, personal communication, 1987) and alkali feldspar granite of presumed Cambrian to Devonian age and a wide variety of granitic to quartz dioritic and syenitic sheets and mafic dykes. Justino and Sangster (1987) were unable to determine the relation between the Lime Hill gneissic complex and the George River Group *sensu stricto*, but postulated the gneissic complex may represent either a deeper level, more severely metamorphosed, less carbonate-rich sequence of George River Group rock types or uplifted, fault-bounded basement to the lower

grade George River Group *sensu stricto*.

Following the detailed mapping and descriptions of Justino (1985, in prep.) and Justino and Sangster (1987) it can no longer be assumed that the agent of metamorphism in the Lime Hill gneissic complex was the heat evolved during the intrusion and crystallization of the associated plutonic rocks. In particular, the extent of gneisses, and the wider distribution of high grade rock types preclude the assignment of the metamorphism as directly contact related. In this study, the petrology of the metamorphic rocks has been investigated with a view to determining the extent, variability, and agent of the metamorphism.

The Lime Hill gneissic complex

The Lime Hill gneissic complex outcrops in two portions of the North Mountain, on the eastern side of the mountain from Ross Brook to Dallas Brook, and on the western side 2 km south of the Big Brook stop on the CNR line (Fig. 2). The larger block is bounded to the north by a northwesterly trending fault which juxtaposes the gneiss against the low grade rocks of the George River Group. Both blocks have been intruded by the Big Brook tonalitic to granodioritic pluton and by the West Bay alkali-feldspar granite (Justino, pers. comm. 1987). In addition, numerous granitoid and mafic dykes occur throughout the gneissic complex. Many of these have been reported to display aureoles up to several centimetres wide, which are best developed in the carbonate rocks where abundant serpentine or massive diopside has formed (Justino and Sangster 1987).

The gneissic complex shows uniformly high metamorphic grade, complex structures and in some areas evidence for anatectic migmatization. Four main lithologies can be distinguished on hand specimen and petrographic criteria. These include biotite gneiss, cordierite-biotite gneiss, amphibolite and a

variety of carbonate-bearing lithologies ranging from calcite marble to multiphase assemblages including forsterite, diopside, tremolite, talc, brucite, periclase, wollastonite, calcite and dolomite. Amphibolite and carbonate-bearing lithologies are subordinate in amount, but the complex structure and limited outcrop have prohibited correlation of these rock types across the gneissic complex.

The typical biotite gneisses are dark, fine to medium grained, well foliated rocks with weakly to moderately developed gneissic layering (Justino and Sangster 1987). Biotite gneisses range from rust-brown weathering pelitic varieties to white weathering quartzofeldspathic varieties. These differences appear to represent variations in biotite content and protolith composition and both types are composed of biotite, quartz, plagioclase (An_{21-48}), and minor opaque minerals. Many of the biotite gneisses contain significant quantities K-feldspar, commonly microcline perthite, and some also contain small quantities of garnet or pyroxene. It is probable that many of the K-feldspar-bearing biotite gneisses represent metamorphosed plutonic rocks, as K-feldspar is very rarely associated with sillimanite, and most of the K-feldspar-bearing rocks contain small quantities of mafic minerals.

Cordierite-biotite gneisses typically are similar in hand specimen appearance to those biotite gneisses rich in biotite. They tend to be rich in mafic minerals, particularly biotite and cordierite, but display moderately to well developed continuous banding on the scale of 1 to 10 mm. Biotite is enriched in the mafic layers and cordierite in the quartzofeldspathic layers, which appear to represent neosomes in a migmatite.

Abundant mafic boudins have been reported from the biotite gneiss (Justino and Sangster 1987). These are highly variable in their mafic content, but universally contain hornblende, plagioclase, quartz and opaque minerals. Justino and Sangster (1987) suggested the amphibolites represent

metamorphosed mafic calc-silicate layers and/or mafic dykes. In this study, the term amphibolite has been restricted to those rocks which are composed mainly of dark green to brown strongly pleochroic hornblende and plagioclase (An_{40-70}), which probably originally were mafic sheets in the gneiss. Other amphibole-bearing lithologies, e.g. rocks containing actinolite or tremolite and calcic plagioclase (An > 70 %) are considered as calc-silicate rocks. One sample of clinopyroxene-bearing amphibolite was noted.

Carbonate-bearing lithologies occur in the central part of the Lime Hill gneissic complex, in the area of the Lime Hill zinc showing. These range from dolomite or calcite marble to siliceous marble and carbonate-bearing calc-silicate rocks. They occur as finely stratified rocks interlayered with the biotite and biotite-cordierite gneisses. Calc-silicate lithologies occur closely associated with the carbonate-rich lithologies and also distributed across the gneissic complex, remote from the areas of known carbonate-rich rock types. These grade into amphibolite and biotite gneiss, and probably represent minor carbonate sedimentation in mafic, pelitic and semipelitic sequences.

Mineral assemblages of the Lime Hill gneissic complex

Biotite gneiss

Biotite gneiss is the most abundant phase in the Lime Hill complex. It occurs in both the eastern and western portions of the complex, and is typically composed of biotite, K-feldspar, plagioclase and quartz, with minor amounts of Fe-Ti oxides and zircon. Accessory tourmaline and apatite is present in many specimens, pyroxenes are present in some samples and garnet is less common (Appendix 1). Many samples are moderately to severely retrograded to sericite-chlorite-quartz assemblages, but in unaltered rocks a well-developed granoblastic texture is preserved.

The gneissic fabric is formed by alternating layers of different biotite contents, but in an individual layer biotite is randomly oriented. Biotite-rich layers are also richer in opaque minerals and quartz. K-feldspar is typically medium to coarse-grained and is restricted to the more leucocratic layers. In most samples it is orthoclase, with a poorly developed perthitic structure, in marked contrast to the dyke phases in the gneissic complex which are non-perthitic microcline. Plagioclase is uniformly distributed throughout the rock, and occurs as poorly twinned, unzoned, xenoblastic crystals. Quartz typically occurs as rounded inclusions or irregular patches in both the leucocratic and biotite-rich layers. Pyroxene was found in several biotite gneisses, and occurs as irregular patches, in some cases concentrated in biotite-rich layers. Hypersthene and augite appear to be equally abundant, although only one specimen was found with both pyroxenes in a calc-silicate-free portion of the rock. Diopside is present in calcium-rich layers in some gneisses. Garnet has been recorded in a few biotite gneisses, but comprises less than 2 % of any sample.

Cordierite-biotite gneiss

Cordierite-biotite gneiss makes up approximately one-third of the quartzofeldspathic rocks examined. It appears to be particularly abundant in the Ross Brook area and in the western portion of the gneissic complex near Big Brook, but it is not possible to delineate zones in which all biotite gneisses contain cordierite, or in which cordierite-biotite gneisses are absent. There is a wide variety of textures displayed by the cordierite-biotite gneisses, including both disrupted and well layered varieties, and migmatitic varieties, some showing phlebitic, stromatic, schlieren, or ophthalmitic structures (after Mehnert 1971).

Cordierite tends to occur in the quartzofeldspathic layers of the

gneisses. In some cases these appear to be leucosomes of migmatites, but in many of the gneisses cordierite occurs in the leucocratic layers of banded rocks which do not preserve clear evidence of anatectic migmatization (e.g. distinct leucosome, melanosome and paleosome, or igneous textures in the leucosome). Cordierite occurs as irregular to tabular, coarse grained patches of xenoblastic grains, and as isolated, medium grained, ovoid crystals. Alteration has variably affected cordierite - in some rocks it has been replaced by fine grained aggregates of muscovite and green biotite, in others it is preserved with minor pinitization on the margins. Commonly associated with the cordierite is sillimanite, as masses of fine grained needles, and increased quantities of Fe-Ti oxides and biotite. Andalusite, spinel and corundum, mantled by cordierite, are present in some samples. Other phases in the cordierite-biotite gneiss are texturally similar to those in the biotite gneiss, although the layering is generally more prominent and more clearly defined, and garnet and sillimanite are found in the groundmass in greater amounts.

Amphibolite

Amphibolite, occurring as boudins in biotite gneiss, contains the assemblage hornblende-plagioclase-quartz-opaque minerals. Biotite is common, and K-feldspar is rarely found. Many amphibolites display well preserved relict igneous textures, particularly zoned plagioclase (some with oscillatory zoning) and diabasic or gabbroic textures. These are referred to as metagabbro and metadiabase in Appendix 1. Such amphibolites are difficult to distinguish from diorites, and some metagabbros may represent foliated dioritic dykes.

A variety of amphibolite, with substantial quantities of biotite, and typically interlayered with biotite gneiss, was encountered across the Lime

Hill gneissic complex. This hornblende-biotite gneiss also rarely contains clinopyroxene or K-feldspar and tends to be depleted in mafic minerals compared to true amphibolites from boudins. It probably represents a concordant sedimentary unit in the gneiss, with a significant mafic component.

Retrograde metamorphism has affected most of the amphibolites. In some rocks hornblende has been retrograded to actinolite-chlorite aggregates, and the plagioclase severely sericitized.

Calcareous and calc-silicate lithologies

Carbonate-bearing and calc-silicate rocks are extremely varied in mineralogy and appearance. Pure calcite marble is rare - most of the samples examined contain forsterite (up to 20 %), commonly partially or completely retrograded to serpentine. Dolomite was encountered in two samples of forsterite-calcite marble. In siliceous marbles, and both carbonate-bearing and carbonate-free calc-silicate rocks, diopside is almost universal, forsterite (with retrograde serpentine), and talc are common, and some samples contain some of spinel, graphite, periclase, brucite, wollastonite, clinozoisite, scapolite, and sphalerite (Appendix 1). Opaque phases include pyrite, pyrrhotite, and chalcopyrite. Chatterjee (1980a) has also reported the occurrence of galena, bornite, covellite, chondrodite, merwinite, monticellite, scheelite, hydrotungstite, and sanmartinite, from the area of the Lime Hill zinc showing, although none of these minerals were noted in this study. Many of these minerals, although characteristic of low pressure contact metamorphism and metasomatism of calcareous rocks, may occur in minor contact and metasomatic aureoles associated with the wide variety of dykes which cut the Lime Hill gneissic complex. Metasomatised calc-silicate lithologies from dyke margins were not examined in this study. They do not appear to be developed in calc-silicate rocks adjacent to the larger plutonic

phases.

Metamorphic petrology

Retrograde metamorphism

All lithologies of the Lime Hill gneissic complex display the effects of retrograde metamorphism, particularly in the area of the Lime Hill zinc showing. The most obvious effects are extensive sericitization of feldspars and alteration of cordierite to fine-grained nearly isotropic mats of mica(?). Extensive alteration to chlorite and epidote is restricted to the mafic lithologies, where hornblende and biotite may be completely replaced, although chloritized biotite is common in all lithologies in the area of the zinc showing. Mafic lithologies also display replacement of hornblende by actinolite. The most obvious effect of retrograde metamorphism in the marbles is the replacement of forsterite by serpentine. This appears to be ubiquitous, and in several samples is complete.

In some biotite and biotite-cordierite gneisses muscovite is present. In almost all cases this muscovite occurs as large irregular plates, associated with feldspar, aluminosilicate minerals or cordierite or as finely intergrown aggregates of biotite and muscovite. It has commonly grown across the boundaries of these minerals and appears to have replaced them. These textural observations indicate the muscovite is entirely retrograde in the Lime Hill gneisses. As muscovite is a typical phase of lower grade pelitic and semipelitic rocks, its absence as a prograde phase implies that metamorphic conditions exceeded those for its decomposition in the presence of quartz and feldspar, which is in the range of 600-700°C, at a $P_{H2O} = P_{TOTAL}$, and pressure of 300-500 MPa (Thompson and Algor 1977).

Andalusite was detected in three samples. In two samples it contains inclusions of magnetite, spinel or corundum and is closely associated with

cordierite. It appears to have formed in these rocks by the breakdown of corundum or spinel, possibly in reaction with cordierite:

$$6\ FeAl_2O_4 + 2\ Fe_2Al_4Si_5O_{18} + 5\ O_2 = 10\ Al_2SiO_5 + 5\ Fe_2O_3.$$

This reaction is an oxidation reaction, and appears to have proceeded under retrograde conditions, resulting in an overall diminution of grain size, and the mantling of corundum and spinel grains by andalusite. Andalusite is also present in sample 86-SFB-350, where it is a minor phase associated with biotite, plagioclase, garnet, sillimanite and quartz. In this situation, the andalusite appears to have formed by the retrograde reaction:

$$\text{sillimanite} = \text{andalusite}.$$

It appears to have nucleated preferentially in biotite-rich layers in the gneiss. All three occurrences of andalusite indicate a significant phase of retrograde metamorphism, sufficiently intense to nucleate and crystallize medium grained andalusite, and coarse grained muscovite and chlorite. Maximum pressure-temperature conditions for such an event appear to have been in the amphibolite facies, at pressures less than 400 MPa (the upper stability of andalusite - Holdaway, 1971), and temperatures less than 600-700°C (the upper stability of the assemblage muscovite + plagioclase + quartz - Thompson and Algor, 1977).

Prograde metamorphism

The major prograde phases which appear to be in textural equilibrium in the maximum assemblage biotite-cordierite gneisses are biotite, cordierite, plagioclase, K-feldspar, quartz, garnet, ilmenite, magnetite and melt (e.g. sample 86-SFB-140). Sillimanite is also present in such rocks, although in every case sillimanite appears to be isolated from cordierite, commonly being enclosed by biotite, plagioclase, garnet and quartz. Using this assemblage it is possible to limit the minimum conditions of peak metamorphism (Fig. 3),

based on the reactions:

andalusite or kyanite = sillimanite (Holdaway 1971)

Al_2SiO_5 + Na-plagioclase + K-feldspar + quartz + H_2O = melt (Thompson and Tracy 1979)

biotite + K-feldspar + quartz + sillimanite + H_2O = melt (Seifert 1976)

biotite + sillimanite + quartz = cordierite + K-feldspar + H_2O (Holdaway and Lee 1977).

Except for the aluminosilicate polymorphic transformation reaction, these reactions are strongly dependent on the water content of the fluid phase. In the Lime Hill area, carbonate rocks are well known, but are abundant only in a relatively small area near the Lime Hill zinc and tungsten showing, and dehydration reactions are prevalent. Carbonate minerals are absent from all analyzed samples. Accordingly, XH_2O is assumed to be 1.0, in the derivation of the P-T diagram (Fig. 3). Lower values of XH_2O would have the effect of decreasing the temperature of the dehydration reactions by up to 100°C. No significant variation in metamorphic grade can be detected across the gneissic complex, based on the assessment of mineral assemblages.

The assemblages sillimanite-garnet-corundum-cordierite and sillimanite-garnet-hercynite-cordierite are also useful in limiting the conditions of the prograde metamorphism. Harris (1981) reported the formation of hercynite spinel and corundum by local desilication during anatexis in biotite-sillimanite-quartz-plagioclase-bearing rocks at temperatures below 720°C. Five samples from the Lime Hill gneissic complex appear to have undergone variable amounts of desilication in the neosomes of the migmatites, and have preserved univariant and divariant assemblages around an invariant point involving garnet, Fe-cordierite, hercynite, sillimanite, corundum and quartz in the Al_2O_3-SiO_2-FeO system (Fig. 3). The position of this invariant point has been calculated at about 650°C, 250 MPa (Harris 1981).

Physical conditions of metamorphism

Eight samples of biotite and cordierite-biotite gneiss were selected for chemical analysis. Seven of these samples contain the assemblage garnet-biotite-sillimanite(± andalusite)-plagioclase-quartz, necessary for the simultaneous determination of metamorphic pressure and temperature conditions based on the the garnet-biotite Fe-Mg exchange reaction and the garnet-Al_2SiO_5-plagioclase-quartz solid exchange reaction. Samples were selected from both outcrop areas of the Lime Hill gneiss and from the area of the Lime Hill zinc showing.

Mineral chemistry

Garnet is highly variable in appearance in the eight analyzed samples, but in all cases except sample 86-SFB-140 prograde or peak metamorphic portions of garnet grains can be recognized. Compositional zoning is pronounced in garnets from three samples (Fig. 4), with the rims being notably richer in the spessartine component and the Mg/(Mg+Fe) ratio being higher in the cores (Appendix 2a). Pyrope content displays an antithetic relationship to almandine and spessartine content, and grossular displays the same relationship in one sample. In samples MJ85-332A and MJ85-354A, the steep compositional gradients are coincident with textural discontinuities, particularly the density and grain size of inclusions, and the cores were probably not in chemical equilibrium with the biotite, plagioclase, sillimanite and quartz of the matrix. In sample 86-SFB-350, the zoning is restricted to a narrow rim with a low Mg/(Mg+Fe) ratio, which appears to be the product of post-metamorphic re-equilibration. Five samples show minimal or no zoning except for minor spessartine enrichment in the rims (Fig. 4). Grossular and spessartine contents are uniformly low, generally less than 5 and 10 mol %, respectively.

Biotite occurs as 1 to 4 mm laths in the groundmass of all samples. In a single sample, biotite compositions are uniform, and no compositional gradients were detected either within individual biotite grains or with distance from garnet grains. In sample MJ-85-700 two generations of biotite are present - a brown phase, with normal concentrations of TiO_2 and a green phase lacking in TiO_2. Texturally, the brown biotite appears to be in equilibrium with garnet and plagioclase, and the green biotite occurs as an intergrowth with quartz, indicative of retrograde metamorphism (Appendix 2b).

Cordierite is unzoned, and generally uniform in composition in any one rock. The range in the Fe/(Fe+Mg) ratio is limited to 0.345 to 0.379. Analytical totals are slightly below 100 %, implying the cordierites are partly hydrated. In all samples, the cordierite is at least partly pinitized, and complete pinitization has occurred in sample MJ85-700 (see analysis on Appendix 2c).

Plagioclase occurs as an anhedral 1 to 6 mm diameter groundmass phase. Many plagioclases show zoning optically, but microprobe analysis of cores and rims commonly reveals less than 5 An % variance. Exceptions are samples MJ-85-700, which ranges from An_{44} to An_{31} (core to rim), and MJ-85-332A, which ranges from An_{48} to An_{22} (irregular distribution). Complete analyses are given in Appendix 2d.

K-feldspar is abundant in the more quartzofeldspathic rocks, where it typically occurs as orthoclase perthite. It is present in at least three of the analyzed rocks, and its orthoclase content ranges from 0.827 to 0.875 (Appendix 2e). It appears to be unzoned.

Geothermometry

Temperature determinations based on five calibrations of the garnet-biotite Fe-Mg exchange reaction are listed in Table 1. The patterns displayed

by the eight samples appear to independent of the calibration used, although the absolute temperatures determined from a single sample vary by up to 174°C. Temperatures have been determined using compositional data from both the rims and cores of zoned garnets in three samples. In samples MJ85-332A and MJ85-354A, biotite-garnet core pairs yield unrealistically high temperatures, supporting the conclusion reached above that the garnet cores were not in equilibrium with the present composition of biotite. In sample 86-SFB-350 the almandine-rich rim yields a significantly lower temperature than the core, indicating that this feature may be a retrograde effect.

Using the calibration of Hodges and Spear (1982) (T5 on Table 1) the range of temperatures recorded by six samples is 730 to 777°C. Sample MJ85-426 yielded a temperature of 868°C, using the Hodges and Spear (1982) calibration, and significantly higher temperatures using the calibrations of Ferry and Spear (1978), Thompson (1976) and Pigage and Greenwood (1982). However, using the Indares and Martignole (1985) calibration, it yields a lower temperature than some other samples. The garnet in this sample appears to be unzoned, but the biotite is largely retrograded, with abundant exsolution of rutile needles. The Indares and Martignole (1985) calibration is the only one which takes into account the possibility of non-ideal mixing of Ti and octahedral Al in biotite, and it is possible that the few large, relatively rutile-free biotite grains in this rock have been affected by alteration or retrograde metamorphism, and that equilibrium cannot be assumed between the biotite and garnet. Garnet-biotite pairs in sample 86-SFB-140 yield relatively low temperatures, although in this case the garnets are partially retrograded to chlorite and sericite and the garnet grains are small, the largest analyzed having a diameter of 0.46 mm. It is likely that the garnet composition represents retrograde re-equilibration of the entire

garnet with biotite, and not the peak metamorphic temperature.

Geobarometry

Pressure was determined from the anorthite-grossular exchange reaction in the assemblage garnet-plagioclase-sillimanite-quartz. Of the eight samples which were used for geothermometry, seven contain sillimanite in the same thin section, and aluminum saturation has been assumed for these. Pressures determined using the calibration of Ghent (1976) range from 335 to 363 MPa, for five of the samples (Table 2). This is a very narrow range, given the uncertainties in the geobarometer, the propagation of analytical uncertainties in the calculation, and the presence of andalusite in some of the samples.

Three pressures were determined which are outside the range of the main cluster. In two cases, these pressures are strongly dependent on the input temperatures, and may be spurious, but in sample 86-SFB-140, the distribution coefficient, log Ks (Table 2), is markedly less negative, and may indicate a real variation in the pressure of equilibration.

Sample 86-SFB-350 is notable, yielding a "normal" temperature and pressure from garnet core analyses, and a lower temperature and pressure from the rim analyses. The lower pressure lies within the andalusite field of Holdaway (1971), and is confirmed by the presence of andalusite in a reaction relationship with cordierite.

Discussion

The gneisses of the Lime Hill gneissic complex have reached metamorphic conditions characteristic of the middle to upper amphibolite facies. In particular, muscovite has been eliminated as a prograde phase, and extensive cordierite-bearing migmatites have developed. Sillimanite is the dominant aluminosilicate polymorph. Migmatization has occurred with associated local desilication, producing corundum or hercynite. These assemblages in the

quartzofeldspathic gneisses occur with forsterite-diopside marble assemblages in calc-silicate rocks and hornblende-clinopyroxene amphibolite assemblages in mafic lithologies. No variation in metamorphic grade can be detected across the two exposure areas of gneiss.

Estimates of the temperature and pressure of metamorphism, based on elemental exchange equilibria between garnet and biotite, and plagioclase and garnet indicate a relatively narrow field of metamorphic conditions, near 750°C and 340 MPa. This range is in agreement with the conditions deduced from analysis of the major mineral assemblages (Fig. 3). The temperatures derived from analysis of the garnet-sillimanite-cordierite-corundum-hercynite system are 70 to 100 °C lower, probably because of the effect of Mg in the cordierite, garnet and spinel.

Retrograde metamorphism has been prevalent in the Lime Hill gneisses. Most notably, there has been extensive development of muscovite, pinitization of cordierite, chloritization of biotite, hornblende and clinopyroxene, and growth of sphene overgrowths on ilmenite. Other retrograde alteration features include the breakdown of cordierite + spinel and cordierite + corundum assemblages to andalusite ± magnetite. Such reactions limit the main phase of retrograde metamorphism to the low pressure region of the lower amphibolite facies.

The inferred pressure-temperature conditions for the gneiss require a geothermal gradient in the order of 80 to 100 °C/km. Such conditions may be attributed to contact metamorphism (as proposed for the Lime Hill area by Chatterjee, 1980a) or by regional thermal perturbations caused by mafic intrusions at shallow depths. However, the uniformity of grade across the entire gneissic complex precludes a direct contact metamorphic origin for the gneisses. No meaningful trends in the geothermometric analysis can be

recognized. All temperatures appear to be within the error limits of the calibration, except for sample MJ85-426, which is the sample farthest from any igneous body. It is more likely that that the agent of metamorphism was heat evolved from the intrusion of a large mafic mass, and which may be related to the Big Brook granodiorite to tonalite pluton which has been identified west of the Lime Hill gneissic complex (Justino and Sangster 1987).

The migmatitic nature of the gneisses is particularly significant, in that the metamorphic conditions must be limited by curves 2 and 3 to pressures lower than 400 MPa and temperatures above 650°C. These conditions are at lower pressures than the intersection of the quartz + muscovite + plagioclase breakdown curve, which is responsible for the derivation of K-feldspar + sillimanite assemblages, with the granitic melt curve (ca. 500 MPa, Tracy 1978), and account for the scarcity of K-feldspar + sillimanite assemblages. The most feasible reaction for the development of migmatite is the biotite breakdown reaction (reaction 3, Fig. 3), which is also responsible for the production of cordierite. The migmatitic leucosomes, therefore, represent anatectic peraluminous granitic melts, some of which may have been extruded from the gneisses and accumulated as granitic magma. The extensive suite of granitic dykes which have intruded the Lime Hill gneissic complex may be derived from this magma, and may have been further responsible for local metamorphism and metasomatism at the contacts of the dykes with the calc-silicate lithologies in the vicinity of the Lime Hill zinc showing. Such local effects can be termed contact metamorphism, and could be responsible for the wide mineralogical variety documented by Chatterjee (1980a).

A phase of dyke intrusion may have been responsible for the extensive retrograde metamorphism observed in many samples from the gneiss, although the significantly lower pressures and temperatures required to stabilize andalusite require a period of uplift prior to the main phase of the

retrograde metamorphism. Alternatively the intrusion of the West Bay alkali feldspar granite may be responsible for this event.

The uniformly high metamorphic grade, and the distinctive low pressure style of metamorphism, distinguish the Lime Hill gneissic complex from other stratified units in the North Mountain area of Cape Breton Island (i.e. the George River Group, *sensu stricto*). The contact between the gneiss and the low grade units is faulted, and it is not possible to correlate one with the other on the basis of this study. The lithological types found in the Lime Hill gneissic complex can be matched to rocks of similar composition in the George River Group, although it appears that the relative abundances are different (Justino and Sangster 1987). Correlation can better be made between the Lime Hill gneissic complex and the Kellys Mountain Gneiss - both of these units are characterized by low pressure upper amphibolite facies metamorphism, with the abundant development of aluminosilicate-bearing cordierite gneisses (andalusite + sillimanite at Kellys Mountain), and cordierite migmatites (Jamieson 1984). Other reports of gneiss in the Bras d'Or Zone of Cape Breton Island include the Boisdale Hills (Barr and Setter 1984) and the Creignish Hills (J. Campbell, in prep.). Such blocks of gneiss may be correlative, although it is premature to compare them without a detailed investigation of the metamorphic development and the chemistry of each one.

Jamieson (1984) invoked heat evolved from the intrusion of dioritic bodies as the agent of metamorphism of the Kellys Mountain Gneiss, and the same may be the case for the Lime Hill gneissic complex. However, the recognition of a number of high grade low pressure gneisses in the Bras d'Or Zone may indicate that a more regional high heat flow event was responsible for the metamorphism, and that the association with dioritic and granodioritic

to tonalitic plutons may be secondary to the original source of the heat, serving mainly to develop "hot spots" within the zone.

The distinctive metamorphic style and wide range of lithologies displayed by the Lime Hill gneissic complex and the Kellys Mountain Gneiss distinguish it from the Grenvillian rocks in northern Cape Breton Island (Barr *et al.* 1987a), suggesting that the Bras d'Or Zone is not underlain by Grenvillian basement. Instead, the gneisses of the Bras d'Or Zone may represent the high temperature, low pressure metamorphism characteristic of the root zone of an oceanic-oceanic or continental-oceanic collisional zone.

Conclusions

1. The Lime Hill gneissic complex has been metamorphosed to low pressure, upper amphibolite facies conditions, as determined from the presence of sillimanite, cordierite-bearing migmatites, and cordierite-K-feldspar and cordierite-corundum assemblages.
2. Using the garnet-biotite geothermometer and the garnet-plagioclase-Al_2SiO_5-quartz geobarometer, peak metamorphic conditions are in the order of 750°C and 350 MPa.
3. Extensive migmatization resulted in the segregation and accumulation of granitic magma as dykes which were intruded into the gneiss and were responsible for local metamorphism and metasomatism where they are in contact with calc-silicate lithologies.
4. Extensive retrograde metamorphism occurred at lower pressure conditions (andalusite stable), possibly near 550°C and 200 MPa. This phase of metamorphism may be associated with the intrusion of the West Bay alkali feldspar granite.
5. The Lime Hill gneissic complex bears many compositional and petrological similarities to the Kellys Mountain Gneiss, with which it appears to

correlate, and may be similar to other gneissic fragments recognized in the Bras d'Or Zone.

6. The metamorphic regime displayed by the Lime Hill gneissic complex and the Kellys Mountain Gneiss is unlike that recognized in the Grenvillian rocks exposed in northwestern Cape Breton Island and Newfoundland, and indicates that the gneisses of the Bras d'Or Zone are not part of the Grenville Province, incorporated in the Appalachian Orogen.

References

Barr, S.M., O'Reilly, G.A. and O'Beirne, A.M.
1982: Geology and geochemistry of selected granitoid plutons of Cape Breton Island; Nova Scotia Department of Mines and Energy, Paper 82-1, 176p.

Barr, S.M. and Raeside, R.P.
1986: Pre-Carboniferous Tectonostratigraphic subdivisions of Cape Breton Island; Maritime Sediments and Atlantic Geology, v. 22, p. 252-263.

Barr, S.M., Raeside, R.P. and Macdonald, A.S.
1985: Geological mapping of the southeastern Cape Breton Highlands, Nova Scotia; *in* Current Research, Part B, Geological Survey of Canada, Paper 85-1B, p. 103-109.

Barr, S.M., Raeside, R.P. and van Breemen, O.
1987a: Grenvillian basement in the northern Cape Breton Highlands, Nova Scotia; Canadian Journal of Earth Sciences, v. 24, p. 992-997.

Barr, S.M., Raeside, R.P., White, C.E. and Yaowanoiyothin, W.
1987b: Geology of the northeastern and central Cape Breton Highlands, Nova Scotia; *in* Current Research, Part A, Geological Survey of Canada, Paper 87-1A, p. 199-207.

Barr, S.M. and Setter, J.R.D.
1984: Petrology of granitoid rocks of the Boisdale Peninsula, central Cape Breton Island, Nova Scotia; Nova Scotia Department of Mines and Energy, Paper 84-1, 75 p.

Bell W.A. and Goranson, E.A.
1938: Bras d'Or map area, Nova Scotia; Geological Survey of Canada, Map 359A.

Chatterjee, A.K.
1977: Tungsten mineralization in the carbonate rocks of the George River Group, Cape Breton Island, Nova Scotia; Nova Scotia Department of Mines, Paper 77-7.

Chatterjee, A.K.
1980a: Mineralization and associated wall rock alteration in the George River Group, Cape Breton Island, Nova Scotia; Ph.D. thesis, Dalhousie University, Halifax, N.S., 197 p.

Chatterjee, A.K.
1980b: Lime Hill zinc-tungsten mineralization; *in* Mineral Deposits and mineralogenic provinces of Nova Scotia, Geological and Mineralogical Associations of Canada, Joint Annual Meeting, Halifax, N.S., Field Trip Guidebook, p. 45-51.

Ferry, J.M. and Spear, F.S.
1978: Experimental calibration of the partitioning of Fe and Mg between biotite and garnet; Contributions to Mineralogy and Petrology, v. 66, p. 113-117.

Ghent, E.D.
1976: Plagioclase-garnet-Al_2SiO_5 - a potential geobarometer-geothermometer; American Mineralogist, v. 64, p. 874-885.

Guernsey, T.D.
1928: Geology of the North Mountain, Cape Breton; Geological Survey of Canada, Summary Report 1927, part C, p. 47-82.

Harris, N.
1981: The application of spinel-bearing metapelites to P/T determinations: an example from south India; Contributions to Mineralogy and Petrology, v. 76, p. 229-233.

Hodges, K.V. and Spear, F.S.
1982: Geothermometry, geobarometry and the Al_2SiO_5 triple point at Mt. Moosilauke, New Hampshire; American Mineralogist, v. 67, p. 1118-1134.

Holdaway, M.J.
1971: Stability of andalusite and the aluminum silicate phase diagram; American Journal of Science, v. 271, p. 97-131.

Holdaway, M.J. and Lee, S.M.
1977: Fe-Mg cordierite stability in high grade pelitic rocks based on experimental, theoretical, and natural observations; Contributions to Mineralogy and Petrology, v. 63, p. 175-198.

Indares, A. and Martignole, J.
1985: Biotite-garnet geothermometry in the granulite facies: the influence of Ti and Al in biotite; American Mineralogist, v. 70, p. 272-278.

Jamieson, R.A.
1984: Low pressure cordierite-bearing migmatites from Kellys Mountain, Nova Scotia; Contributions to Mineralogy and Petrology, v. 86, p. 309-320.

Justino, M.F.
1985: Geology and petrogenesis of the plutonic rocks of North Mountain, Cape Breton Island; Nova Scotia Department of Mines and Energy, Information Series, v. 9, p. 111.

Justino, M.F.
in preparation: M.Sc.. thesis, Acadia University, Wolfville, Nova Scotia.

Justino, M.F. and Sangster, A.L.
1987: Geology in the vicinity of the lIme Hill zinc occurrence, southwestern Cape Breton Island, Nova Scotia; *in* Current Research, Part A, Geological Survey of Canada, Paper 87-1A, p. 555-561.

Kelley, D.G.
1967: Baddeck and Whycocomagh map-areas; Geological Survey of Canada, Memoir 351, 65 p.

Keppie, J.D.
1979: Geological map of the Province of Nova Scotia, 1:500 000 scale; Nova Scotia Department of Mines and Energy.

Mehnert, K.R.
1971: Migmatites and the origin of granitic rocks; Elsevier, Amsterdam, 405 p.

Milligan, G.C.
1970: Geology of the George River Series, Cape Breton; Nova Scotia Department of Mines and Energy, Memoir 7, 111p.

Pigage, L.C. and Greenwood, H.J.
1982: Internally consistent estimates of pressure and temperature: the staurolite problem; American Journal of Science, v. 282, p. 943-969.

Raeside, R.P. and Barr, S.M.
1986: Stratigraphy and structure of the southeastern Cape Breton Highlands, Nova Scotia; Maritime Sediments and Atlantic Geology, v. 22, p. 264-277.

Raeside, R.P. and Barr, S.M.
1987: Geological map of the igneous and metamorphic rocks of northern Cape Breton Island; Geological Survey of Canada, Open File 1594, 10 sheets, scale 1:50 000.

Raeside, R.P., Barr, S.M. and Jong, W.
1984: Geology of the Ingonish River-Wreck Cove area, Cape Breton Island, Nova Scotia; Nova Scotia Department of Mines and Energy, Report 85-1, p. 249-258.

Raeside, R.P., Barr, S.M., White, C.E. and Dennis, F.A.R.
1986: Geology of the northernmost Cape Breton Highlands, Nova Scotia; *in* Current Research, Part A, Geological Survey of Canada, Paper 86-1A, p. 291-296.

Seifert, F.
1976: Stability of the assemblage cordierite + K-feldspar + quartz; Contributions to Mineralogy and Petrology, v. 57, p. 179-185

Thompson, A.B.
1976: Mineral reactions in pelitic rocks: II. Calculation of some P-T-X(Fe-Mg) phase relations; American Journal of Science, v. 276, p. 425-454.

Thompson, A.B. and Tracy, R.J.
1979: Model systems for anatexis of pelitic rocks: II, Facies series melting and reactions in the system CaO-$KAlO_2$-$NaAlO_2$-Al_2O_3-SiO_2-H_2O; Contributions to Mineralogy and Petrology, v. 70, p. 429-438.

Thompson, A.B. and Algor, J.R.
1977: Model system for anatexis of pelitic rocks: I. Theory of melting reactions in the system $KAlO_2$-$NaAlO_2$-Al_2O_3-SiO_2-H_2O; Contributions to Mineralogy and Petrology, v. 63, p. 247-269.

Tracy, R.J.
1978: High grade metamorphic reactions and partial melting in pelitic schist, west-central Massachusetts; American Journal of Science, v. 278, p. 150-178.

Wiebe, R.A.
1972: Igneous and tectonic events in northeastern Cape Breton Island, Nova Scotia; Canadian Journal of Earth Sciences, v. 9, p. 1262-1277.

FIGURE CAPTIONS

Figure 1. Location of the Lime Hill Gneiss and tectonostratigraphic subdivisions of Cape Breton Island (after Barr and Raeside 1987).

Figure 2. Geology of the Lime Hill gneissic complex (after Justino and Sangster 1987, Justino in preparation) and sample locations of analyzed rocks.

Figure 3. P-T diagram with results for analyzed gneisses (filled triangles), using the garnet-biotite calibration of Hodges and Spear (1982) and the anorthite-grossular calibration of Ghent (1976). Labelled reactions : 1, muscovite + albite + quartz = K-feldspar + Al_2SiO_5 + H_2O, (Thompson and Tracy 1979); 2, Al_2SiO_5 + albite + K-feldspar + quartz + H_2O = melt, (Thompson and Tracy 1979); 3, biotite + Al_2SiO_5 + quartz = cordierite (30 mol % Fe) + K-feldspar + H_2O, (Holdaway and Lee 1977); 4, biotite + K-feldspar + quartz + sillimanite + H_2O = melt, (Seifert 1976). Dashed lines are univariant reactions in the Al_2O_3-SiO_2-FeO system (Harris 1981), A = almandine, Cn = corundum, Co = Fe-cordierite, He = hercynite spinel, Si = sillimanite. For all water-evolving reactions, P_{H2O} is assumed to equal P_{total}.

Figure 4. Zoning profiles of selected garnets from eight samples of biotite or biotite-cordierite gneiss. Axes are labelled in mol %. alm = almandine, gro = grossular, pyr = pyrope, spe = spessartine. The distance across the garnet grain (generally the largest grain in the thin section) is indicated in the upper right corner of each graph.

TABLE CAPTIONS

Table 1. Garnet-biotite geothermometry.

Table 2. Garnet-biotite-sillimanite-quartz geobarometry.

APPENDICES

Appendix 1. Mineral assemblages of the Lime Hill gneissic complex.

Appendix 2. Mineral analyses.
- 2a. Garnet analyses.
- 2b. Biotite analyses.
- 2c. Cordierite analyses.
- 2d. Plagioclase analyses.
- 2e. K-feldspar analyses.

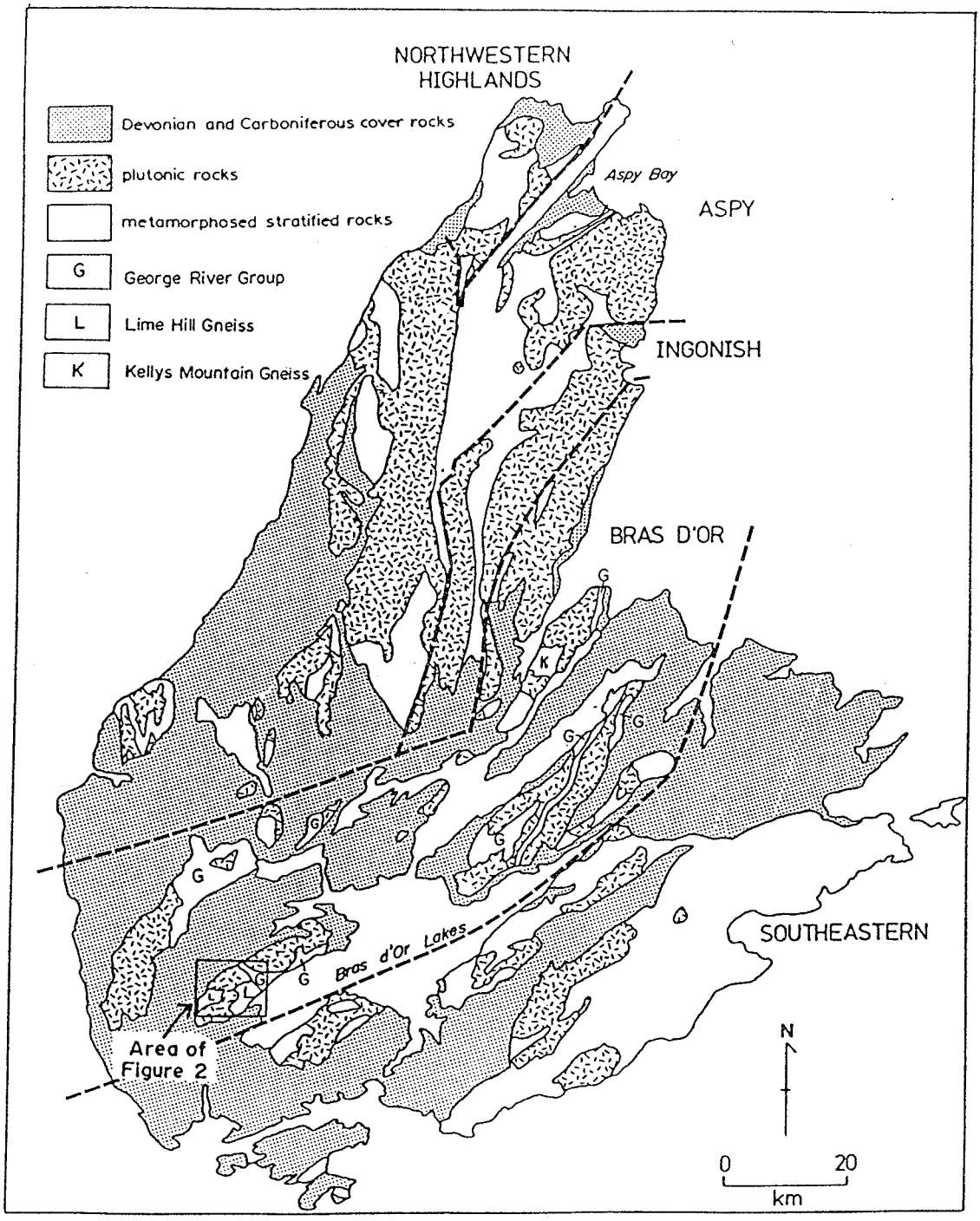
NORTHWESTERN
HIGHLANDS
Devonian and Carboniferous cover rocks
plutonic rocks
metamorphosed stratified rocks
G George River Group
L Lime Hill Gneiss
K Kellys Mountain Gneiss
Aspy Bay
ASPY
INGONISH
BRAS D'OR
SOUTHEASTERN
Bras d'Or Lakes
Area of
Figure 2
N
0
20
km

Figure 1

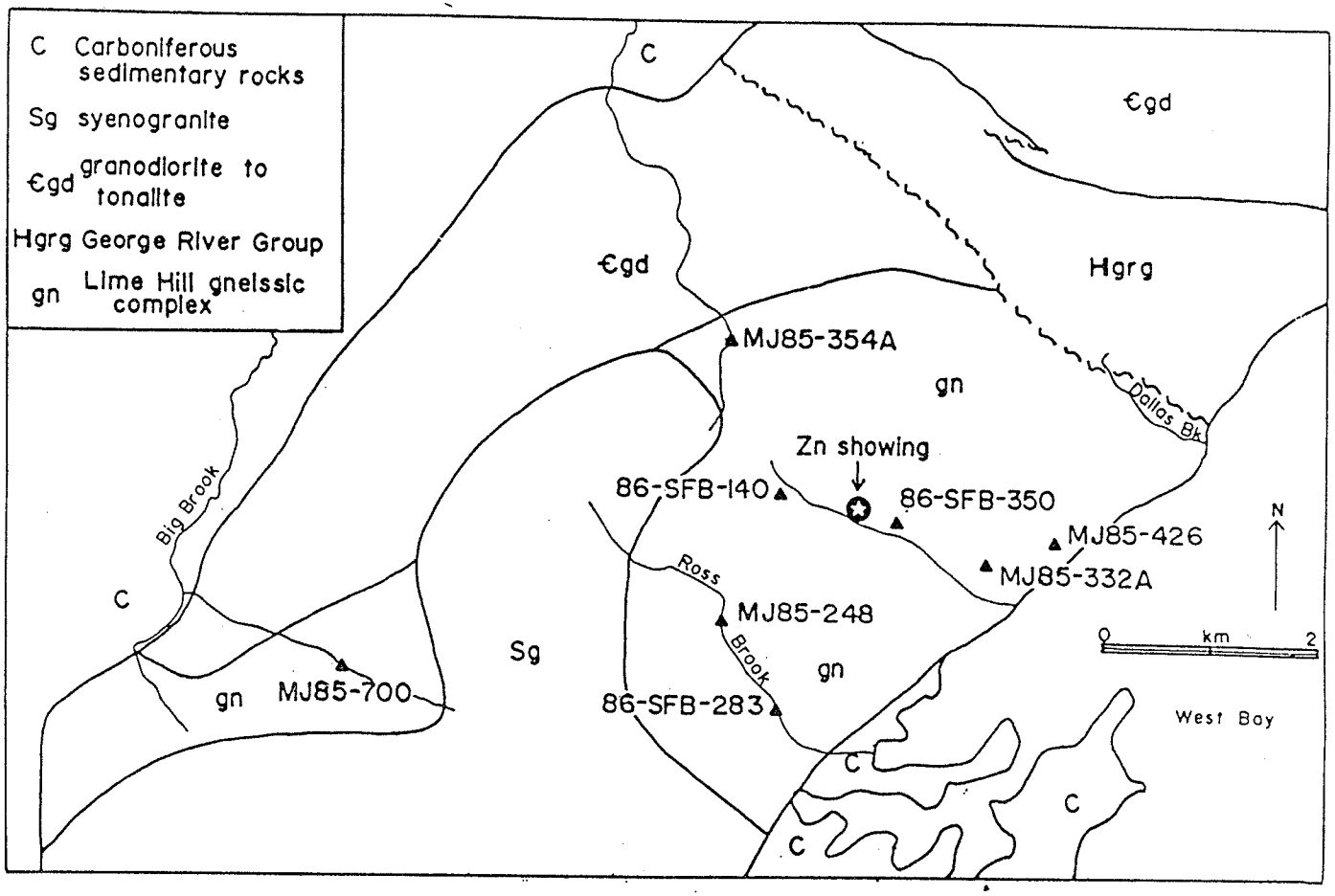
C Carboniferous sedimentary rocks
Sg syenogranite
€gd granodiorite to tonalite
Hgrg George River Group
gn Lime Hill gneissic complex
C
€gd
Hgrg
MJ85-354A
gn
Dallas Bk.
Zn showing
86-SFB-140
86-SFB-350
MJ85-426
MJ85-332A
Big Brook
Ross
Brook
MJ85-248
Sg
gn
MJ85-700
86-SFB-283
West Bay
N
0
km
2

Figure 2

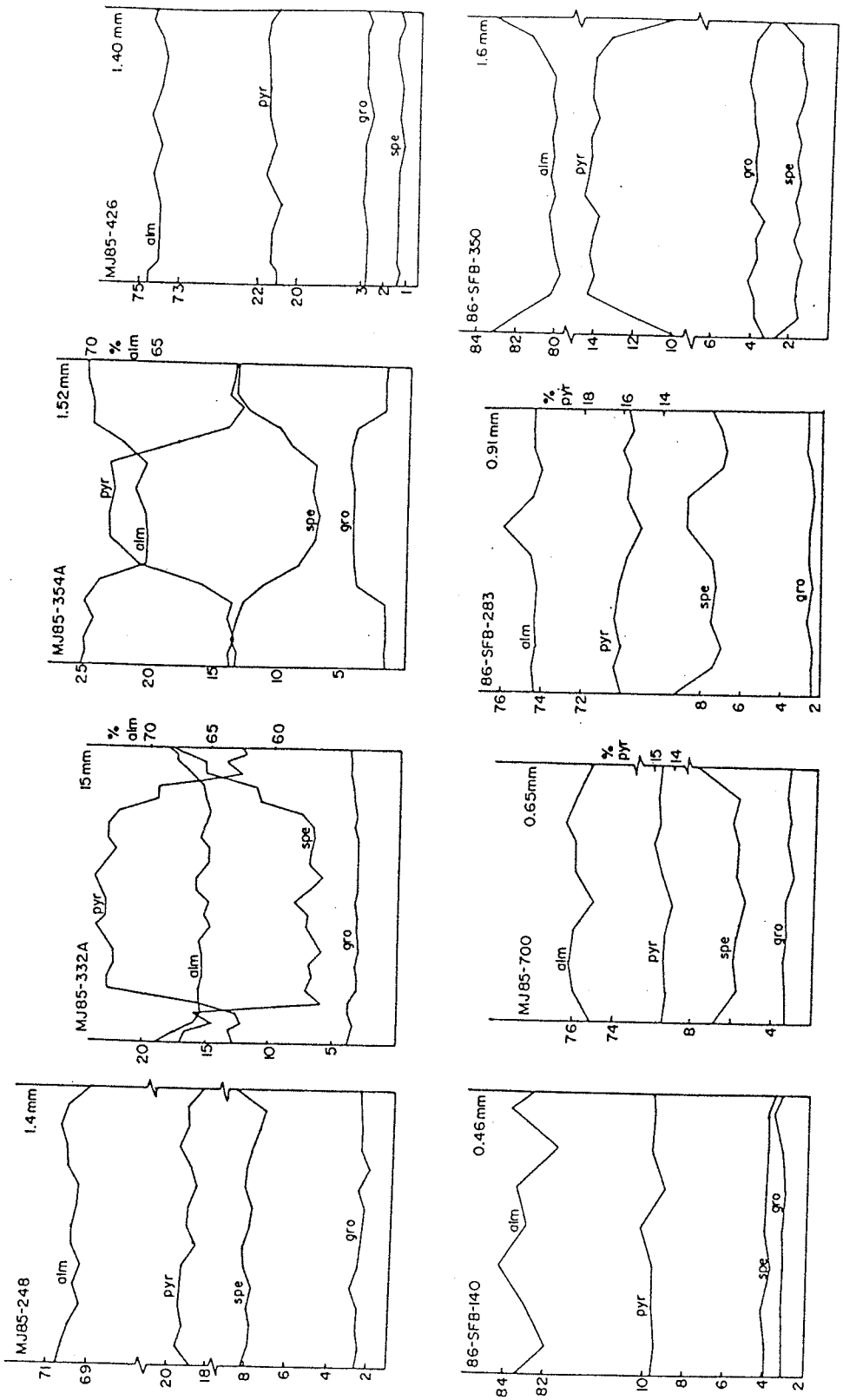
MJ85-248
1.4mm
alm
pyr
spe
gro
MJ85-332A
1.5mm
MJ85-354A
1.52mm
MJ85-426
1.40mm
86-SFB-140
0.46mm
MJ85-700
0.65mm
86-SFB-283
0.91mm
86-SFB-350
1.6mm
% alm
% pyr

Figure 3

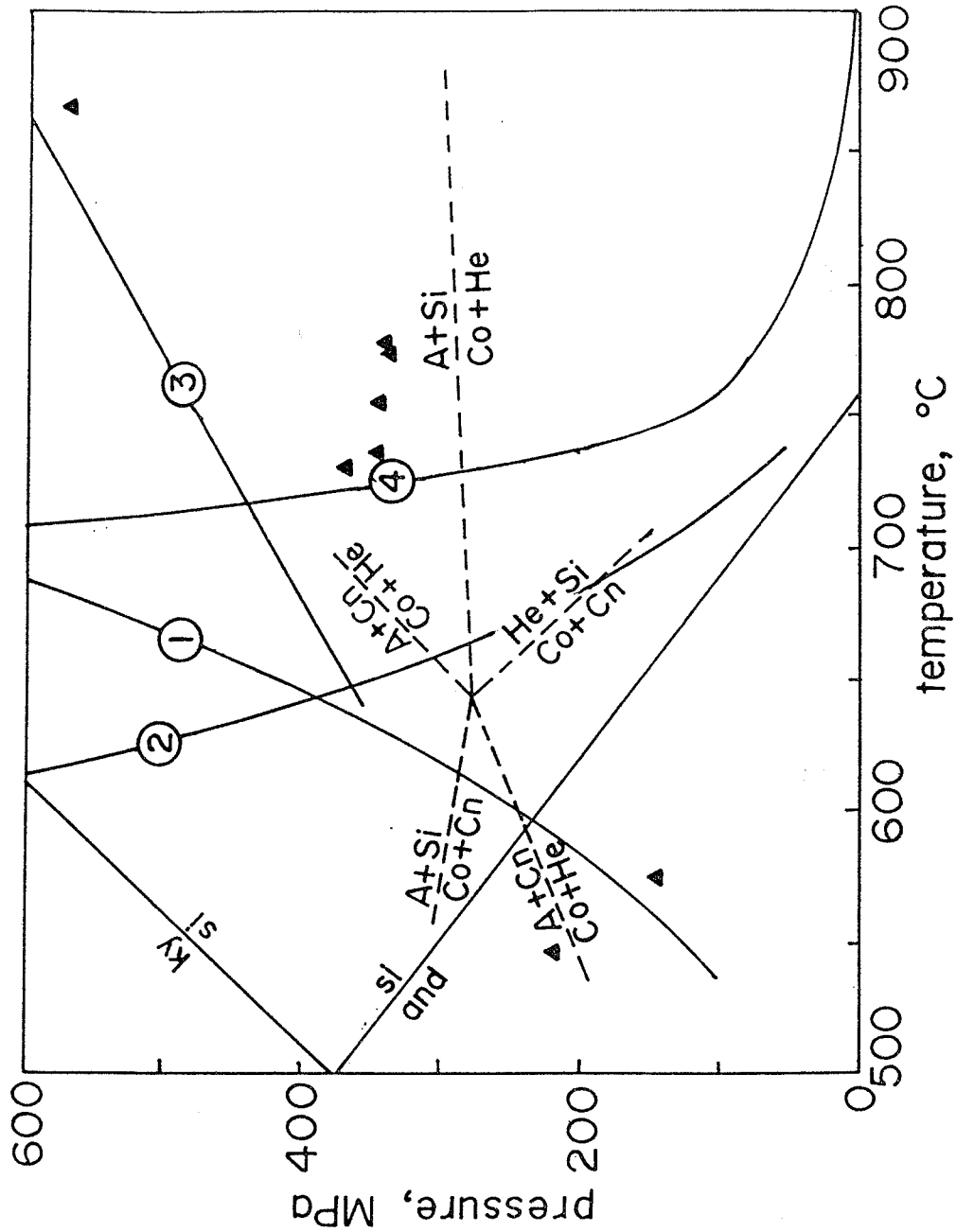
pressure, MPa
temperature, °C
600
400
200
0
500
600
700
800
900
ky
si
and
si
A+Si
Co+Cn
A+Cn
Co+He
A+Si
Co+He
He+Si
Co+Cn
Cn+He
+Co
A+O
1
2
3
4

Table 1. Garnet-biotite geothermometry.

Sample	Mg/Fe gar	Mg/Fe biot	X_{gt} Ca	X_{gt} Mn	X_{bi} Ti	X_{bi}^{vi} Al	T1	T2	T3	T4	T5
MJ85-248	.276	.991	.025	.081	.057	.123	764	734	835	691	776
MJ85-332A c	.367	.760	.041	.068	.036	.054	1143	976	1244	1132	1178
MJ85-332A r	.191		.041	.154			715	698	838	768	732
MJ85-354A c	.358	.760	.041	.068	.066	.082	1120	962	1220	1023	1154
MJ85-354A r	.197		.016	.143			730	709	829	696	736
MJ85-426	.284	.867	.027	.013	.045	.154	853	795	884	731	868
MJ85-700	.194	.699	.032	.058	.072	.121	763	732	824	650	777
86-SFB-140	.115	.730	.031	.040	.057	.139	540	565	578	456	548
86-SFB-283	.213	.794	.023	.076	.058	.135	746	720	810	661	756
86-SFB-350 c	.180	.719	.039	.016	.042	.151	703	697	751	622	730
86-SFB-350 r	.122		.037	.027			563	584	600	491	574

Table 2. Garnet-biotite-sillimanite-quartz geobarometry.

Sample	Xgro	Xalm	Xpyr	Xspe	Xan	log Ks	P, MPa
85-248	.025	.700	.193	.081	.348	-3.431	335
85-332A rim	.041	.675	.129	.154	.351	-3.205	363
85-426	.027	.747	.212	.013	.295	-3.115	570
85-700	.032	.762	.148	.058	.445	-3.430	337
86-140	.031	.834	.096	.040	.295	-2.935	210
86-283	.023	.742	.158	.076	.298	-3.337	346
86-350 core	.039	.801	.144	.016	.473	-3.251	345
86-350 rim	.037	.834	.102	.027	.473	-3.320	131

Appendix 1. Mineral assemblages in rocks from the Lime Hill Gneissic Complex.
(Samples supplied by M. Justino and A. Sangster).

BIOTITE GNEISSES AND BIOTITE-CORDIERITE GNEISSES

Sample	Lithology	qz	pl	kf	mu	bi	as	gt	co	cx	ox	hb	tr	ep	ch	to	zr	sp	ap	op	cc	cd	sn	other	Approximate location
MJ-85-132	co gneiss	x	x		s	x			x									x	x	x	2				MacKenzies Little B
MJ-85-135	bi gneiss	x	x	p	s	x									2		x			x					MacKenzies Little B
MJ-85-136	co gneiss	x	x	m	s	x			x						2		x			x					MacKenzies Little B
MJ-85-229	orthogneiss	x	x		s	x								x	2										Ross Bk
MJ-85-242	co gneiss	x	x		s	x			x					2	2			x		x					Ross Bk
MJ-85-248	co gneiss	x	x		s	x	as		x						2		x	x	x	impr		x		sc	Ross Bk
MJ-85-278	co gneiss	x	x	pm	s	x			x										x	x					MacCuspics Bk
MJ-85-305	orthogneiss	x	x	x	2	x									2					x					Big Bk
MJ-85-308	bi gneiss	x	x			x									2					x					Big Bk
MJ-85-331	orthogneiss	x	x			x									2					x					MacPhees Bk
MJ-85-332A	orthogneiss	x	x			x	f	x							2	x			x	mp					MacPhees Bk
MJ-85-333	co gneiss	x	x		2	x			x								x			x				gf	MacPhees Bk
MJ-85-354A	orthogneiss	x	x	p		x		x							2					x					McIntyre Bk
MJ-85-355	gneiss	x	x		s	x									2					x					McIntyre Bk
MJ-85-423	bi gneiss	x	x	s	2										2					x					Ross Bk area
MJ-85-424	gneiss	x	x		s									2	2			2							Ross Bk area
MJ-85-424A	gneiss	x	x		s									2	2			2							Ross Bk area
MJ-85-424B	gneiss	x	x		s								a	2	2		x	x		x					Ross Bk area
MJ-85-426	co gneiss	x	x		2	x	s	x	x						2		x			im		x			Lime Hill road
MJ-85-505	gneiss	x	x	m		x								2	2					x					Big Bk
MJ-85-506	co gneiss	x	x		2	x			x					2	2					x	2				Big Bk
MJ-85-507	gneiss	x	x		s	x								2	2		x			x					Big Bk
MJ-85-700	co gneiss	x	x	x		x	f	x	x					2		x	x			mpr					Big Bk
86-SFB-132	gneiss	x	x	p	2	x													x	x					grid W
86-SFB-138	bi schist	x	x			x							a2	2						x					grid NW
86-SFB-140	co migmatite	x	x	mp		x	f	x	x								x		x	im		he			grid NW
86-SFB-149	co gneiss	x	x	p		x			x						2					x					grid SE
86-SFB-157	px migmatite	x	x		2	x				x			a2							x					grid SE
86-SFB-184	co migmatite	x	x		2	x	s		x											x					grid SW
86-SFB-193	orthogneiss	x	x			x					x			2	2		x		x	x					grid NE
86-SFB-213	bi migmatite	x	x			x				x					2					x					grid NE
86-SFB-219	granulite	x	x		2				x					2	2					x					MacKenzies Little B
86-SFB-220	bi gneiss	x	x		s	x									2					x					MacKenzies Little B
86-SFB-223	px-bi gneiss	x	x		2	x			x											x					MacKenzies Little B
86-SFB-225	orthogneiss	x	x	m	2	x									2				x	x					MacKenzies Little B
86-SFB-227	px gneiss	x	x	m	2	x					x		a2		2										MacKenzies Little B
86-SFB-235	bi gneiss	x	x	x	2	x								2	2		x			x					grid NW
86-SFB-236A	bi gneiss	x	x		2	x		x							2		x			x					grid NW
86-SFB-245	px migmatite	x	x	m		x				x	x	x			2					x					Dallas Lakes
86-SFB-246	co migmatite	x	x		s	x			x						2					x					Dallas Lakes
86-SFB-253	px migmatite	x	x		s	x					x					x	x		x	x					Dallas Lakes Bk
86-SFB-255	co gneiss	x	x	m		x			x									x	x	x					Dallas Lakes Bk
86-SFB-256	gneiss	x	x	m	s	x								2	2			x	x	x					Dallas Lakes Bk
86-SFB-273	co gneiss	x	x		s	x		x	x											x					grid SE
86-SFB-276B	orthogneiss	x	x	x		x								2	2		x			x					MacPhee Bk

Sample Lithology qz pl kf mu bi as gt co cx ox hb tr ep ch to zr sp ap op cc cd sn other

Sample	Lithology	qz	pl	kf	mu	bi	as	gt	co	cx	ox	hb	tr	ep	ch	to	zr	sp	ap	op	cc	cd	sn	other	
86-SFB-278	gneiss	x	x		s	x									2				x						Ross Bk
86-SFB-280	migmatite	x	x	m	2	x					x								x						Ross Bk
86-SFB-283	co migmatite	x	x		2	x	af		x						2		x		ip		x	Zh			Ross Bk
86-SFB-286	co gneiss	x	x			x			x										x						Ross Bk
86-SFB-287	orthogneiss	x	x	x	s	x								2	2		x		x						Ross Bk
86-SFB-289	altered rock	x	x		s	x								2	2				x						Ross Bk
86-SFB-299	px gneiss	x	x			x					x								x						Ross Bk
86-SFB-321A	gneiss	x	x		s	x													x						grid W
86-SFB-350	co migmatite	x	x		2	x	as		x	x							x		cimp		x				grid NW
86-SFB-363	px gneiss	x	x	x	s	x						x	x		x	2	2		x						grid SE
86-SFB-384	co migmatite	x	x			x		s	x	x							x		x						grid NE
86-SFB-395	gneiss	x	x	mp	s	x										2			x						MacPhee Bk
86-SFB-408	co migmatite	x	x		s	x		s	x	x							x		x						MacPhee BK
86-SFB-413	gneiss	x	x		s	x										2			x						north of grid
86-SFB-423	bi gneiss	x	x			x							a2						x		x				north of grid
																									grid NW

ap apatite
as aluminosilicate (s = sillimanite, f = fibrolite)
bi biotite
cc calcite (2 = secondary)
cd corundum
ch chlorite (2 = secondary)
co cordierite
cx clinopyroxene
ep epidote (2 = secondary)
gt garnet
hb hornblende
kf K-feldspar (m = microcline, p = perthite)
mu muscovite (s = sericite, 2 = secondary)
op opaque minerals (c = chalcopyrite, i = ilmenite, m = magnetite, p = pyrite, r = rutile)
ox orthopyroxene
pl plagioclase
qz quartz
sp sphene
sn spinel (he = hercynite, Zh = zincian hercynite)
to tourmaline
tr tremolite (a = actinolite, 2 = secondary)
zr zircon
other: gf = graphite, sc = scapolite

AMPHIBOLITES AND OTHER AMPHIBOLE-BEARING ROCKS

Sample	Lithology	qz	pl	kf	mu	bi	gt	hb	tr	cx	ep	ch	cc	to	zr	sp	ap	op	pr	Approximate location
MJ-85-216	amphibolite	x	x		s			x			x					x		x		Ross Bk
MJ-85-221	granodiorite	x	x		s	x		x			x	2				x				Ross Bk
MJ-85-222	hb-bi gneiss	x	x			x		x									x	x		Ross Bk
MJ-85-244	px-hb gneiss	x	x		s	x		x		x					x	x	x	im		Ross Bk
MJ-85-245	diorite	x	x		s	x		x										x		Ross Bk
MJ-85-249	metadiabase		x		s	x		x			2					x	x	x		Ross Bk
MJ-85-273B	metagabbro	x	x		s	x		x				2	x				x	x	x	MacCuspics Bk
MJ-85-314	granulite	x	x	m						x						x	x	x		Big Bk area
86-SFB-121A	greenstone	x	r		x						x	x						x		grid SW
86-SFB-135A	amphibolite		x					x			2	2						x		grid NW
86-SFB-152	amphibolite	x	x	x		x		x										x		grid SE
86-SFB-177	amphibolite	x	x			x		x										x		grid NE
86-SFB-212	hb-bi gneiss	x	x		s	x		x		x								x		grid N
86-SFB-236B	hb-bi gneiss	x	x			x		x								x	x	x		grid NW
86-SFB-252	amphibolite	x	x		s			x										x		Dallas Bk
86-SFB-269A	metagabbro	x	x			x		x			x						x	x		MacCuspics Bk
86-SFB-269B	metagabbro	x	x			x		x			x						x	x		MacCuspics Bk
86-SFB-270	metagabbro	x	x		s	x		x								x	x	x		MacCuspics Bk
86-SFB-285	metagabbro	x	x			x		x				2				x	x	x		Ross Bk
86-SFB-380	diorite		x			x		x									x	x		grid NE

ap apatite
bi biotite
cc calcite (2 = secondary)
ch chlorite (2 = secondary)
cx clinopyroxene
ep epidote (2 = secondary)
gt garnet
hb hornblende
kf K-feldspar
mu muscovite (s = sericite, 2 = secondary)
op opaque minerals (i = ilmenite, m = magnetite)
pl plagioclase
pr prehnite
qz quartz
sp sphene
to tourmaline
tr tremolite
zr zircon

CALC-SILICATE AND CARBONATE ROCKS

Sample	Lithology	cc	do	qz	pl	Kf	ph	tc	tr	di	fo	wo	gr	se	ep	sl	sn	sc	bc	pc	sp	ap	op	Approximate location
MJ-85-251	fo marble	x									x						x		x	x				Ross Bk
MJ-85-310	calc-silicate	x				x	x			x													x	Big Bk area
MJ-85-323A	di marble	x							x	x													x	MacPhee Bk
MJ-85-326	calc-silicate	x		x		x	b			x					cz						x		x	MacPhee Bk
MJ-85-426B	calc-silicate	x			x	m				x			x		cz						x			Lime Hill road
86-SFB-124A	calc-silicate	x	x	x	x		b	x		x			x									x	x	grid SW
86-SFB-126	marble	x	x											x					x					grid SW
86-SFB-136	marble	x	x								x			x										grid NW
86-SFB-161	fo marble	x												x		x							x	grid SE
86-SFB-163	fo marble	x			x		x				x						x							grid SE
86-SFB-170	calc-silicate				x		x		x	x								x					x	grid NE
86-SFB-180	metasom c-sil	x		x	x	mp			x	x														grid W
86-SFB-181	calc-silicate				x		x		x														x	grid SW
86-SFB-187	fo marble	x									x												x	grid NE
86-SFB-188	calc-silicate				x		b			x		x												grid NE
86-SFB-191A	serp marble	x												x									x	grid NE
86-SFB-192	fo marble	x			x						x			x									x	grid N
86-SFB-195	calc-silicate	x							x	x											x		x	grid NE
86-SFB-226	calc-silicate	x		x	x	x			x	x											x	x	x	MacKenzies Little Bk
86-SFB-237	calc-silicate	x								x													x	Dallas Lakes
86-SFB-250	marble	x							x							x				x				grid SE
86-SFB-310	serp marble	x						o	x			x	x	x						x		mp		grid N
86-SFB-319	calc-silicate								x	x	x													grid NE
86-SFB-338	di-tr marble	x								x														grid NW
86-SFB-439	diopside rock									x				x									x	drill-hole
86-SFB-S28	serp marble	x							x			x		x										drill-hole
86-SFB-S29	fo marble	x							x			x												

ap apatite
bc brucite
cc calcite
di diopside
do dolomite
ep epidote (cz = clinozoisite)
fo forsterite
gr grossular
Kf K-feldspar (m = microcline, o = orthoclase, p = perthite)
op opaque minerals (m = magnetite, p = pyrite)
pc periclase
ph phlogopite (b = biotite)
pl plagioclase
qz quartz
sc scapolite
se serpentine
sl sphalerite
sn spinel
sp sphene
tc talc
tr tremolite
wo wollastonite

MISCELLANEOUS ROCKS

Sample	Lithology	qz	pl	kf	mu	bi	co	cx	hb	ep	ch	sp	ap	op	Approximate location
MJ-85-133	granite	x	x	m	s	x					2				MacKenzies Little Bk
MJ-85-240	andesite	x	x		s						2			2	Ross Bk
86-SFB-123	granite dyke	x	x	m		x				x	2	2		x	grid SW
86-SFB-130A	cx-syenite		x	mp				x	2				x	x	x grid W
86-SFB-150	granodiorite	x	x	?	s	x								x	grid SE
86-SFB-173B	granite dyke	x	x	o		x					2				grid NE
86-SFB-194	sheared gran	x	x	m	s2	x				2	2		x	x	
86-SFB-240	pegmatite	x		mp		x									grid SE
86-SFB-256	granite	x	x	m	x	x					2			x	Dallas Bk
86-SFB-259	slate	x	x		x	x	x							x	George River Group
86-SFB-307	granite	x	x	m						2	2	x		x	grid SE
86-SFB-321C	mafic dyke	x	x		s	x		x	x	2	2			x	grid NE

ap apatite
bi biotite
ch chlorite (2 = secondary)
co cordierite
cx clinopyroxene
ep epidote (2 = secondary)
hb hornblende (2 = secondary)
kf K-feldspar (m = microcline, o = orthoclase, p = perthite)
mu muscovite (s = sericite)
op opaque minerals (2 = secondary)
pl plagioclase
qz quartz
sp sphene

Appendix 2.

All mineral analyses were determined using the JEOL 733 Superprobe electron microprobe at the Dalhousie Regional Electron Microprobe Laboratory, Halifax. Analyses were made by wavelength dispersive techniques, using an accelerating voltage of 15 kV, emission current of 250 x 10^{-6} amp, beam current of 0.25 to 0.3 x 10^{-6} amp, and a beam diameter of about 1.5 x 10^{-6} m. Counts were gathered over 10 to 20 second intervals, elements being analyzed sequentially using automated spectrometer drive. Numbers in brackets are one standard deviation variations from the mean.

Appendix 2a. Garnet analyses.

Sample	MJ85-248	MJ85-332A	MJ85-332A	MJ85-354A	MJ85-354A
Site		core	rim	core	rim
n	4	5	3	5	4
SiO_2	37.65 (.62)	38.27 (.10)	37.03 (.16)	37.25 (.38)	37.78 (.52)
TiO_2	.05 (.02)	.06 (.02)	.08 (.01)	.08 (.03)	.07 (.02)
Al_2O_3	21.48 (.28)	22.63 (.14)	22.01 (.06)	21.55 (.22)	22.00 (.20)
Cr_2O_3	.07 (.02)	.06 (.01)	.07 (.01)	.06 (.01)	.08 (.02)
FeO	31.36 (.38)	29.54 (.49)	29.84 (.00)	29.74 (.09)	29.78 (.19)
MnO	3.58 (.42)	3.06 (.53)	6.74 (.47)	3.06 (.66)	5.99 (.68)
MgO	4.86 (.29)	6.08 (.42)	3.20 (.61)	5.99 (.45)	3.29 (.11)
CaO	.88 (.17)	1.45 (.21)	1.43 (.25)	1.44 (.22)	.53 (.10)
Na_2O	.05 (.01)	.05 (.02)	.06 (.00)	.04 (.01)	.05 (.01)
K_2O	.00	.00	.00	.00	.00
Total	99.98	100.18	100.43	99.21	99.57
Almandine	.700	.652	.675	.656	.703
Spessartine	.081	.068	.154	.068	.143
Pyrope	.193	.239	.129	.235	.138
Grossular	.025	.041	.041	.041	.016
Mg/(Mg+Fe)	.216	.268	.160	.264	.165

Sample	MJ85-426	MJ85-700	86-SFB-140	86-SFB-283	86-SFB-350	86-SFB-350
Site					core	rim
n	6	5	5	5	3	3
SiO_2	37.93 (.47)	36.78 (.55)	37.00 (.30)	38.90 (.42)	37.94 (.30)	37.70 (.20)
TiO_2	.08 (.02)	.06 (.02)	.08 (.01)	.05 (.01)	.10 (.02)	.05 (.01)
Al_2O_3	22.18 (.25)	21.47 (.24)	21.55 (.13)	22.60 (.28)	22.00 (.26)	21.71 (.32)
Cr_2O_3	.08 (.01)	.07 (.01)	.15 (.02)	.07 (.02)	.15 (.01)	.12 (.03)
FeO	33.26 (.48)	35.04 (.56)	36.06 (.14)	30.77 (.75)	35.58 (1.17)	36.25 (.50)
MnO	.59 (.04)	2.64 (.41)	1.70 (.19)	3.12 (.44)	.69 (.12)	1.18 (.11)
MgO	5.30 (.28)	3.82 (.29)	2.33 (.20)	3.68 (.41)	3.59 (.97)	2.49 (.49)
CaO	.94 (.02)	1.15 (.10)	1.03 (.03)	.75 (.05)	1.36 (.09)	1.24 (.01)
Na_2O	.06 (.01)	.05 (.01)	.05 (.03)	.04 (.01)	.06 (.01)	.02 (.02)
K_2O	.00	.00	.06 (.02)	.02 (.02)	.06 (.01)	.00
Total	101.42	100.52	100.00	99.25	101.50	100.72
Almandine	.747	.762	.834	.742	.801	.834
Spessartine	.013	.058	.040	.076	.016	.027
Pyrope	.212	.148	.096	.158	.144	.102
Grossular	.027	.032	.031	.023	.039	.037
Mg/(Mg+Fe)	.221	.163	.103	.176	.152	.109

Appendix 2b. Biotite analyses.

Sample	MJ85-248	MJ85-332A	MJ85-354A	MJ85-426
n	4	4	4	6
SiO_2	34.13 (.64)	29.55 (1.12)	34.64 (.40)	34.89 (.75)
TiO_2	2.86 (.68)	1.93 (.83)	3.25 (.26)	2.27 (1.10)
Al_2O_3	19.26 (.28)	19.55 (.61)	17.05 (.31)	20.40 (1.13)
Cr_2O_3	.07 (.02)	.04 (.02)	.07 (.01)	.22 (.16)
FeO	18.53 (.73)	24.23 (1.20)	21.14 (.74)	19.32 (.38)
MnO	.39 (.08)	.54 (.25)	.64 (.04)	.12 (.04)
MgO	10.30 (1.46)	10.33 (.53)	9.02 (.46)	9.40 (.53)
CaO	.05 (.02)	.42 (.39)	.05 (.02)	.04 (.02)
Na_2O	.23 (.07)	.07 (.06)	.20 (.01)	.28 (.06)
K_2O	8.35 (.68)	8.62 (.39)	9.24 (.46)	9.31 (.38)
Total	94.17	95.28	95.30	96.25
Fe/(Mg+Fe)	.502	.568	.568	.536
XTi	.057	.036	.066	.045
XAl^{vi}	.123	.054	.082	.154

Sample	MJ85-700 (brown)	MJ85-700 (green)	86-SFB-140	86-SFB-283	86-SFB-350
n	3	3	5	5	5
SiO_2	34.75 (.13)	35.24 (.09)	35.08 (.65)	34.69 (.37)	35.04 (.68)
TiO_2	3.53 (.04)	.98 (.08)	2.81 (.31)	2.89 (.40)	2.10 (.48)
Al_2O_3	18.67 (.05)	19.19 (.27)	19.01 (.49)	19.39 (.16)	19.06 (.58)
Cr_2O_3	.13 (.01)	.11 (.01)	.14 (.04)	.15 (.02)	.22 (.12)
FeO	20.61 (.11)	19.79 (.18)	20.39 (.16)	19.82 (.57)	20.72 (1.38)
MnO	.30 (.02)	.35 (.05)	.11 (.02)	.19 (.04)	.17 (.03)
MgO	8.09 (.07)	10.26 (.08)	8.35 (.14)	8.83 (.21)	8.36 (.70)
CaO	.04 (.00)	.07 (.01)	.06 (.01)	.05 (.01)	.06 (.02)
Na_2O	.26 (.01)	.31 (.01)	.20 (.07)	.26 (.07)	.32 (.03)
K_2O	9.48 (.03)	9.40 (.38)	9.39 (.37)	9.38 (.23)	9.40 (.28)
Total	95.84	95.69	95.54	95.60	96.09
Fe/(Mg+Fe)	.588	.520	.578	.557	.582
XTi	.072	.019	.057	.058	.042
XAl^{vi}	.121	.139	.139	.135	.151

Appendix 2c. Cordierite analyses

Sample	MJ85-426	MJ85-700	86-SFB-140	86-SFB-283	86-SFB-350
n	3	2	3	4	4
SiO_2	47.79 (1.13)	41.54	48.74 (.25)	48.72 (.35)	48.86 (.12)
TiO_2	.02 (.01)	.02	.05 (.01)	.04 (.00)	.04 (.01)
Al_2O_3	34.72 (.50)	32.82	33.33 (.02)	33.24 (.28)	33.50 (.20)
Cr_2O_3	.00	.08	.07 (.02)	.07 (.01)	.07 (.01)
FeO	7.67 (.11)	3.35	8.11 (.34)	7.97 (.51)	8.56 (.96)
MnO	.23 (.06)	.16	.13 (.01)	.37 (.05)	.25 (.03)
MgO	8.17 (.12)	2.51	8.07 (.10)	8.10 (.28)	7.86 (.58)
CaO	.04 (.01)	.51	.03 (.01)	.03 (.01)	.05 (.01)
Na_2O	.42 (.13)	.24	.21 (.01)	.23 (.05)	.37 (.06)
K_2O	.00	4.77	.02 (.02)	.04 .01	.05 (.01)
Total	99.03	85.99	98.73	98.81	99.60
Fe/(Fe+Mg)	.345	nd	.361	.356	.379

Appendix 2d. Plagioclase analyses

Sample	MJ85-248	MJ85-332A	MJ85-354A	MJ85-426
n	3	5	4	4
SiO_2	59.08 (.60)	59.23 (2.56)	63.12 (.18)	60.37 (.33)
TiO_2	.00	.00	.02 (.01)	.05 (.04)
Al_2O_3	26.51 (.38)	25.94 (1.65)	24.49 (.11)	26.42 (.27)
Cr_2O_3	.00	.00	.00	.00
FeO	.11 (.06)	.09 (.04)	.06 (.02)	.09 (.07)
MnO	.02 (.02)	.02 (.02)	.07 (.01)	.05 (.02)
MgO	.00	.00	.00	.00
CaO	7.43 (.47)	7.43 (1.98)	4.40 (.06)	6.23 (.25)
Na_2O	7.65 (.28)	7.58 (1.07)	8.83 (.18)	8.22 (.14)
K_2O	.07 (.03)	.03 (.01)	.38 (.08)	.00
Total	100.85	100.27	101.32	101.42
An	.348	.351	.211	.295
Ab	.648	.648	.767	.705
Or	.004	.002	.022	.000
		(range of An % = 22 to 48)		

Sample	MJ85-700 core	MJ85-700 rim	86-SFB-140	86-SFB-283	86-SFB-350
n	5	2	3	3	3
SiO_2	55.61 (.74)	60.04	61.01 (.33)	60.55 (.73)	55.32 (.33)
TiO_2	.05 (.00)	.04	.05 (.01)	.05 (.02)	.05 (.03)
Al_2O_3	27.49 (.74)	25.13	24.88 (.40)	25.36 (.16)	27.81 (.22)
Cr_2O_3	.07 (.01)	.05	.02 (.02)	.06 (.01)	.06 (.01)
FeO	.11 (.01)	.11	.09 (.04)	.13 (.03)	.11 (.03)
MnO	.09 (.03)	.08	.06 (.01)	.06 (.01)	.09 (.01)
MgO	.02 (.01)	.00	.01 (.00)	.00	.00
CaO	9.62 (.64)	6.68	6.34 (.41)	6.53 (.31)	10.25 (.31)
Na_2O	6.46 (.23)	8.11	8.26 (.20)	8.37 (.37)	6.23 (.12)
K_2O	.24 (.13)	.13	.19 (.05)	.19 (.02)	.13 (.02)
Total	99.76	100.37	100.90	101.31	100.05
An	.445	.311	.295	.298	.473
Ab	.541	.682	.695	.692	.520
Or	.013	.007	.011	.010	.007

Appendix 2e. K-feldspar analyses.

Sample	MJ85-354A	MJ85-700	86-SFB-140
n	4	4	4
SiO_2	64.73 (.08)	65.35 (.35)	66.00 (.71)
TiO_2	.00	.08 (.01)	.04 (.01)
Al_2O_3	19.51 (.14)	19.25 (.09)	18.99 (.18)
Cr_2O_3	.00	.07 (.02)	.07 (.02)
FeO	.07 (.01)	.09 (.06)	.08 (.02)
MnO	.02 (.01)	.11 (.02)	.02 (.01)
MgO	.00	.02 (.01)	.00
CaO	.08 (.04)	.11 (.01)	.29 (.21)
Na_2O	1.38 (.14)	1.86 (.15)	.29 (.21)
K_2O	15.13 (.25)	13.96 (.39)	13.09 (1.88)
Total	100.89	100.87	101.03
Or	.875	.827	.766
Ab	.121	.167	.220
An	.004	.005	.014